

Biaxial cyclic deformation of an epoxy resin: Experiments and constitutive modeling

Z. XIA, X. SHEN, F. ELLYIN*

Department of Mechanical Engineering, University of Alberta, Edmonton, Alberta, Canada T6G 2G8

E-mail: fernand.ellyin@ualberta.ca

Biaxial (proportional and non-proportional) cyclic tests were conducted on thin-walled tubular specimens to investigate deformation behavior of an epoxy resin, Epon 826/Epi-Cure Curing Agent 9551. The focus was placed on the biaxial stress-strain response and their dependency on the load control mode, stress or strain range and loading path. Experimental results indicated that under strain-controlled equi-biaxial (proportional) cyclic loading, mean stress relaxation occurred in both axial and hoop directions, whereas under stress-controlled equi-biaxial cyclic loading, ratcheting strains accumulated in both principal directions. Under strain- or stress- controlled non-proportional cyclic loading, anisotropy in stress-strain responses was induced in both axial and hoop directions, and the axial and hoop hysteresis loops rotated in opposite directions. This was particularly evident at high stress or strain levels. The experimental results were further used to evaluate the predictive capabilities of a nonlinear viscoelastic constitutive model. Qualitative and quantitative comparison with the test data indicated a good agreement in predicting the complex stress-strain response under biaxial cyclic loading with various loading paths, applied stress or strain ranges and loading control modes. © 2005 Springer Science + Business Media, Inc.

1. Introduction

Polymers and polymeric composites have become an important class of materials in engineering applications. Structures such as pressure vessels, piping and aircrafts, components like mountain bicycle frames and crankshafts are typical examples. In their service life, they are likely subjected to multiaxial stress state with complex loading histories and paths, and in many cases, loading is of a cyclic nature. Therefore, an adequate understanding of the deformation and failure behavior of polymeric materials is a prerequisite for an efficient design and optimal material utilization.

Due to the complex nonlinear viscoelastic nature of polymers, numerical simulations such as finite element method have been extensively used in the stress and deformation analyses of structures made of these materials. However, the reliability of such numerical predictions is highly dependent on the accuracy of the material's constitutive model used in the analysis [1, 2]. Hence the development and verification of constitutive models is a matter of practical significance, and has attracted considerable research efforts in recent years, see e.g. refs. [3–7].

The material to be studied in this investigation is Epon 826/Epi-Cure Curing Agent 9551, a bisphenol-A epoxy resin and a non-MDA (methylene dianiline) polyamine system suitable for high performance com-

posite parts manufactured by filament winding or resin transfer moulding. This epoxy system was chosen because it provides high strength, elongation and toughness, and therefore, is an appropriate matrix for high performance composite materials. The deformation behavior of this epoxy resin when subjected to quasi-static multiaxial loading and uniaxial cyclic loading, can be found in our previous investigations [8, 9].

Although there have been numerous papers published concerning the multiaxial cyclic loading behavior of metals and alloys [10–12], the influence of such a loading condition on polymers has not been fully investigated. Experimental investigations on polymer behavior under cyclic loading were reported in refs. [13–16]. However, almost all of these investigations were for uniaxial cyclic tests on thermoplastic polymers. To the best of our knowledge, experimental data on the multiaxial cyclic deformation behavior of thermosetting polymers have not been reported in the open literature.

It is the objective of this paper to present experimental data of the aforementioned epoxy resin under biaxial proportional and non-proportional cyclic loading conditions. The focus of the study is on the stress-strain response in axial and hoop directions and their dependency on the load control mode, stress or strain range and loading path. A viscoelastic constitutive model recently developed by Xia *et al.* [3] is briefly reviewed

*Author to whom all correspondence should be addressed.



Figure 1 Geometry of tubular specimen with aluminum end tabs.

and used to simulate the experimental results. It will be seen later on that the constitutive model is capable of predicting the complex stress-strain response and simulating most experimental observations under biaxial cyclic loading both qualitatively and quantitatively.

2. Test set-up

2.1. Specimen and testing equipment

Thin-walled tubular specimens were used in this investigation. The procedure for the casting and preparation of specimens can be found in ref. [9]. Aluminum end tabs were glued to the tube ends so that the specimen can be inserted into the gripping system of the test machine without damaging the specimen extremities during the gripping process. Fig. 1 shows the geometry of the tubular specimen with the aluminum end tabs.

All experiments were performed in a servo-controlled electro-hydraulic system, a modified MTS system. The system is capable of applying axial force; internal and external pressure separately or simultaneously. Thus, uniaxial or biaxial stress state can be generated in the specimen. Detailed description of the test system can be found in [17]. The strains were measured using in-house manufactured axial and diametral extensometers.

2.2. Experimental program and testing procedure

The experimental program consisted of biaxial proportional (equi-biaxial) and non-proportional cyclic tests. Thin-walled tubular specimens were subjected to axial loading and internal pressure following predetermined strain or stress cyclic paths. The loading conditions for each type of test are summarized in Table I.

For the proportional (equi-biaxial) cyclic tests with mean stresses or mean strains, the specimens were first loaded biaxially to the mean stress or mean strain level and then cyclic testing commenced. In addition, a triangular waveform was adopted in both channels (axial and hoop) for the proportional cyclic tests.

In the case of non-proportional cyclic loading, the test started from a stress-free (virgin) state. A quarter-circle sectorial non-proportional cyclic loading path was employed. The loading path and the corresponding input signals for axial and hoop directions are depicted in Fig. 2. The stress or strain waves can be represented by:

$$I_a = \begin{cases} A \sin\left(\frac{3\pi}{2}\omega t\right), & \left(\frac{n}{\omega} \leq t < \frac{2}{3\omega} + \frac{n}{\omega}\right) \\ 0, & \left(\frac{2}{3\omega} + \frac{n}{\omega} \leq t < \frac{n+1}{\omega}\right) \\ & n = 0, 1, 2, 3, \dots \end{cases} \quad (1)$$

$$I_h = I_a\left(t - \frac{\pi}{2}\right) \quad (2)$$

where I_a and I_h refer to the axial and hoop input signal, respectively. A is the amplitude of the stress or strain, ω is the frequency of oscillation and t is the time.

The loading rates for the tests were selected in a range that they allowed for the manifestation of the time-dependent behavior of the material yet avoided the excessive heating of the specimen during cycling. All the tests were conducted at room temperature under the laboratory environment. For most cyclic tests, the stress-strain hysteresis loops were recorded for the initial 10 cycles after which they were recorded at each 10 cycles interval until the specimen failure.

3. Test results

3.1. Proportional (equi-biaxial) cyclic loading under strain-control

Strain-controlled equi-biaxial cyclic tests were conducted with two different strain ranges, $\Delta\varepsilon_a = \Delta\varepsilon_h = 1.5\%$ and $\Delta\varepsilon_a = \Delta\varepsilon_h = 3\%$. A strain rate of $1.2 \times 10^{-4} \text{ s}^{-1}$ in both axial and hoop directions was adopted for these two tests. Figs 3a, b and 4a, b show the experimental stress-strain loops, respectively. For comparative purpose, the hysteresis loop of the first cycle and that of $N = 15$ (last recorded cycle prior to specimen

TABLE I Loading conditions of the test program

Loading path	Control mode	Stress or strain range	Mean stress or strain	Loading rate or frequency
Proportional (equi-biaxial)	Strain control	1.5%	0.75%	$1.2 \times 10^{-4} \text{ s}^{-1}$
		3%	1.5%	$1.2 \times 10^{-4} \text{ s}^{-1}$
	Stress control	40 MPa 60 MPa	20 MPa 30 MPa	0.24 MPa/s 0.32 MPa/s
Non-proportional	Strain control	1.5%	0.75%	0.004 Hz
		3%	1.5%	0.002 Hz
	Stress control	40 MPa 60 MPa	20 MPa/s 30 MPa/s	0.004 Hz 0.002 Hz

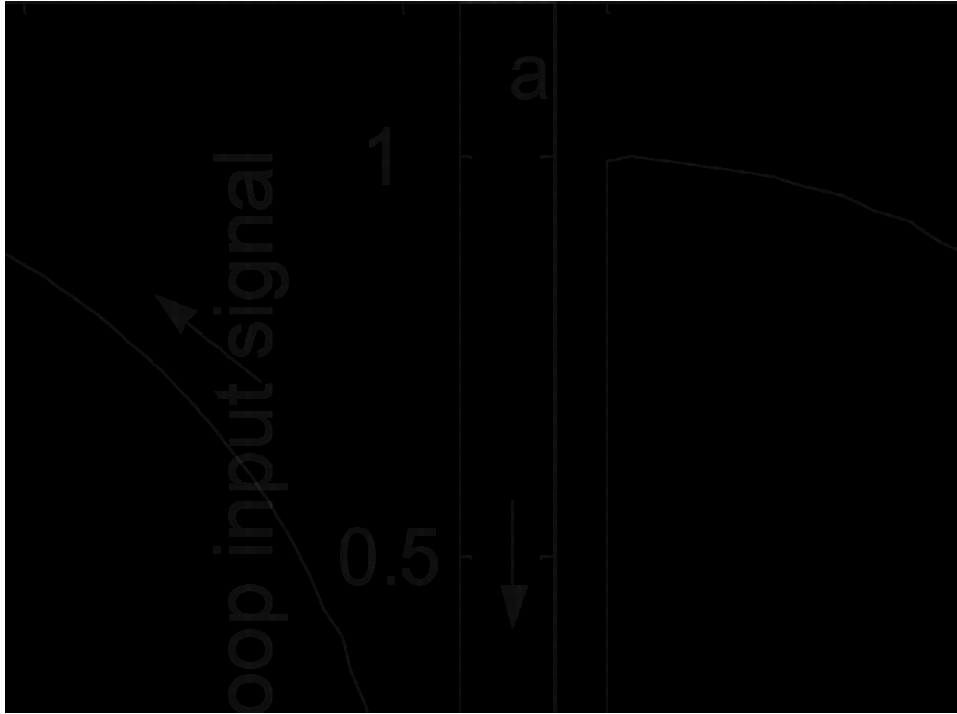


Figure 2 Non-proportional loading path and the corresponding input signals for axial and hoop directions: (a) quarter-circle sectorial cyclic loading path, (b) axial input signal wave and (c) hoop input signal wave.

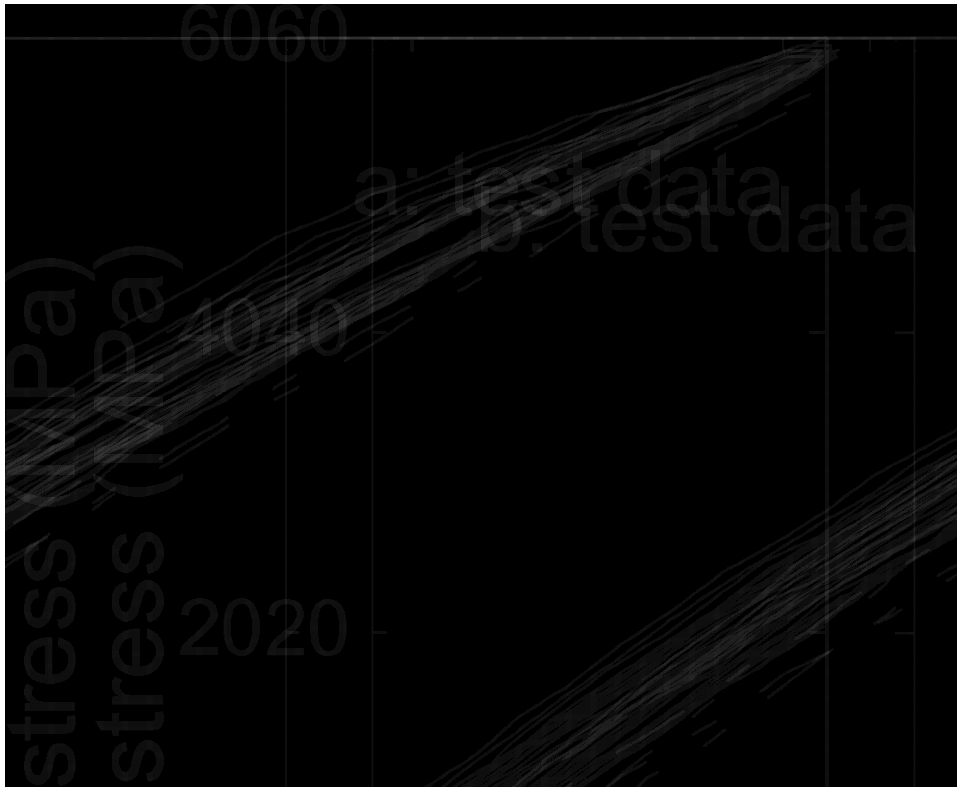


Figure 3 Strain-controlled proportional (equi-biaxial) cyclic loading with strain range of $\Delta\epsilon_a = \Delta\epsilon_h = 1.5\%$: (a) experimental axial stress-strain response, (b) experimental hoop stress-strain response, (c) predicted axial stress-strain response and (d) predicted hoop stress-strain response.

failure) for the large strain range test ($\Delta\epsilon_a = \Delta\epsilon_h = 3\%$) are depicted in Figs 5a and b.

From these test results, we see that the hysteresis loops in the axial and hoop directions, as to be expected, are almost similar, indicating an isotropic property of the material. With the small strain range, Figs 3a and b, the stress-strain loops exhibit an insignifi-

cant amount of nonlinear response and the specimen failed after 120 cycles. With the increasing number of cycles, the hysteresis loops became slimmer. This phenomenon is particularly evident with the higher strain range of 3%, Figs 4a and b, which exhibited pronounced nonlinear response. One observed that the difference the hysteresis loop of $N = 15$ was a much slimmer

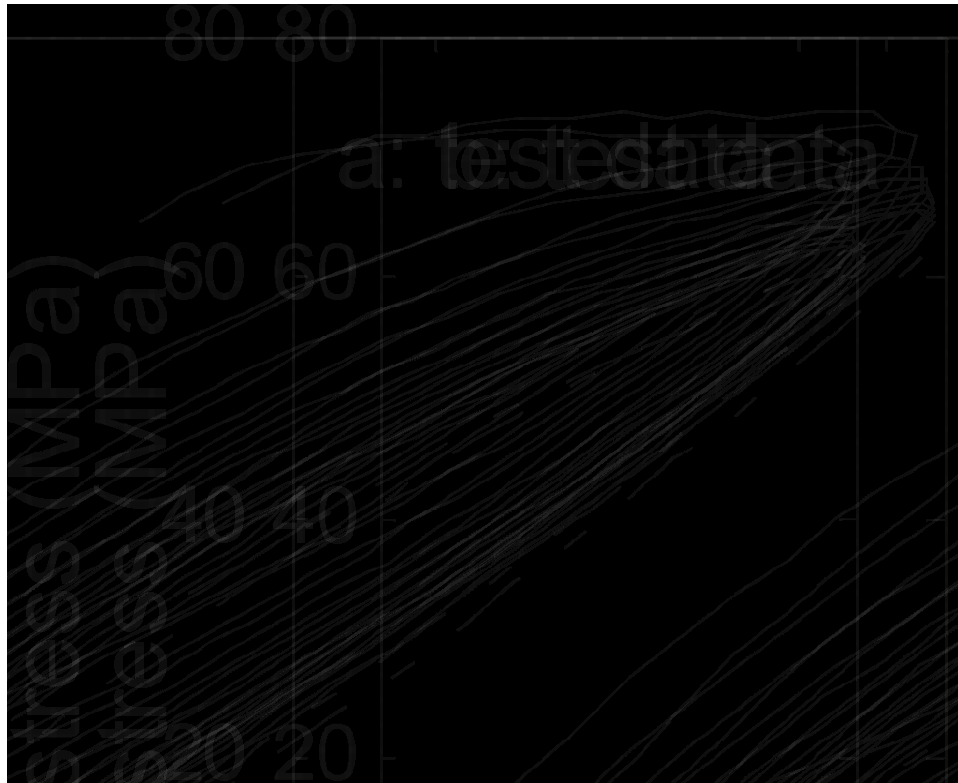


Figure 4 Strain-controlled proportional (equi-biaxial) cyclic loading with strain range of $\Delta\varepsilon_a = \Delta\varepsilon_h = 3\%$: (a) experimental axial stress-strain response, (b) experimental hoop stress-strain response, (c) predicted axial stress-strain response and (d) predicted hoop stress-strain response.



Figure 5 The first and the fifteenth stress-strain loops of the strain-controlled proportional (equi-biaxial) cyclic loading with strain range of $\Delta\varepsilon_a = \Delta\varepsilon_h = 3\%$: (a) experimental axial stress-strain loops, (b) experimental hoop stress-strain loops, (c) predicted axial stress-strain loops and (d) predicted hoop stress-strain loops.

and less nonlinear hysteresis loop prior to specimen failure compared to that of the initial cycle, c.f. Figs 5a and b. For both tests, a mean stress relaxation occurred in both axial and hoop directions. With the increasing number of cycles, the mean stress appeared

to approach an asymptotic value, indicating the attainment of a stable cyclic state. However, the magnitude of mean stress reduction is significantly different for the two tests. In the case of the small strain range of $\Delta\varepsilon_a = \Delta\varepsilon_h = 1.5\%$, the mean stress drop was

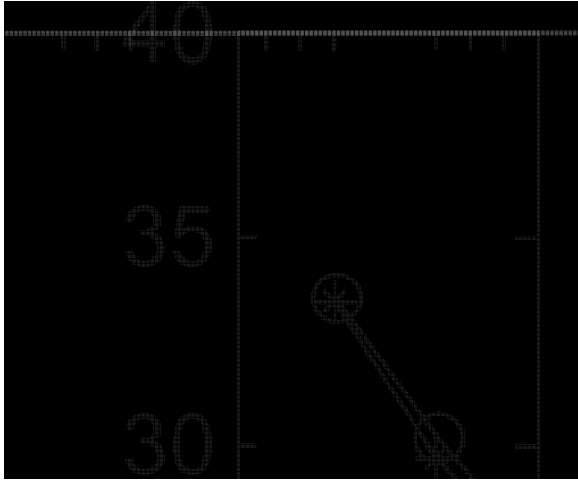


Figure 6 Mean stress relaxation vs. number of cycles for the strain-controlled proportional (equi-biaxial) cyclic loading with strain range of $\Delta\varepsilon_a = \Delta\varepsilon_h = 3\%$. Asterisk solid line: axial mean stress relaxation. Circle solid line: hoop mean stress relaxation.

approximately 4 MPa during the entire cycling process, while for the higher strain range of $\Delta\varepsilon_a = \Delta\varepsilon_h = 3\%$, the mean stress was reduced by 12 MPa from approximately 34 MPa at the first cycle to about 22 MPa at $N = 15$ (prior to fracture), c.f. Fig. 6.

3.2. Proportional (equi-biaxial) cyclic loading under stress-control

Further stress-controlled equi-biaxial cyclic tests were performed with two different stress ranges, $\Delta\sigma_a = \Delta\sigma_h = 40$ MPa and $\Delta\sigma_a = \Delta\sigma_h = 60$ MPa. The stress

rates were chosen to achieve an approximate strain rate of $1.2 \times 10^{-4} \text{s}^{-1}$ for the two tests. The stress-strain curves of these tests are shown in Figs 7a, b and 8a, b. Again, the first hysteresis loop, that of the stable cyclic state and the one prior to the specimen fracture were depicted in Figs 9a and b for the sake of comparison.

For both tests, it was observed that the ratcheting deformation (cyclic creep) accumulated in both axial and hoop directions from the onset of cyclic loading, but in a decreasing rate with the increasing number of cycles. After certain number of cycles ($N = 200$ for the small stress range of $\Delta\sigma_a = \Delta\sigma_h = 40$ MPa, and $N = 60$ for the large stress range of $\Delta\sigma_a = \Delta\sigma_h = 60$ MPa), the ratcheting rate tended to zero and a saturated stress-strain response was attained. It was also noticed that during the cycling process, the slope of the hysteresis loops in both axial and hoop directions did not decrease appreciably, i.e. the stiffness reduction was very small.

In comparing the stress-strain loops with two different stress ranges, it was observed that the higher the stress range, the higher is the accumulated ratcheting strain. For the large stress range of $\Delta\sigma_a = \Delta\sigma_h = 60$ MPa, the ratcheting strain at stable cyclic state reached approximately 0.5%, while it was less than 0.1% for the small stress range of $\Delta\sigma_a = \Delta\sigma_h = 40$ MPa. It is seen from Figs 7a and b that with the small stress range, the hysteresis loops are almost linear in shape throughout the test. The nonlinear stress-strain response was more pronounced for the applied stress range of 60 MPa in both principal directions, as shown in Figs 8a and b. From Figs 9a and b, one can also observe the difference between the stress-strain curves at the first cycle and that at the stable cyclic state. That

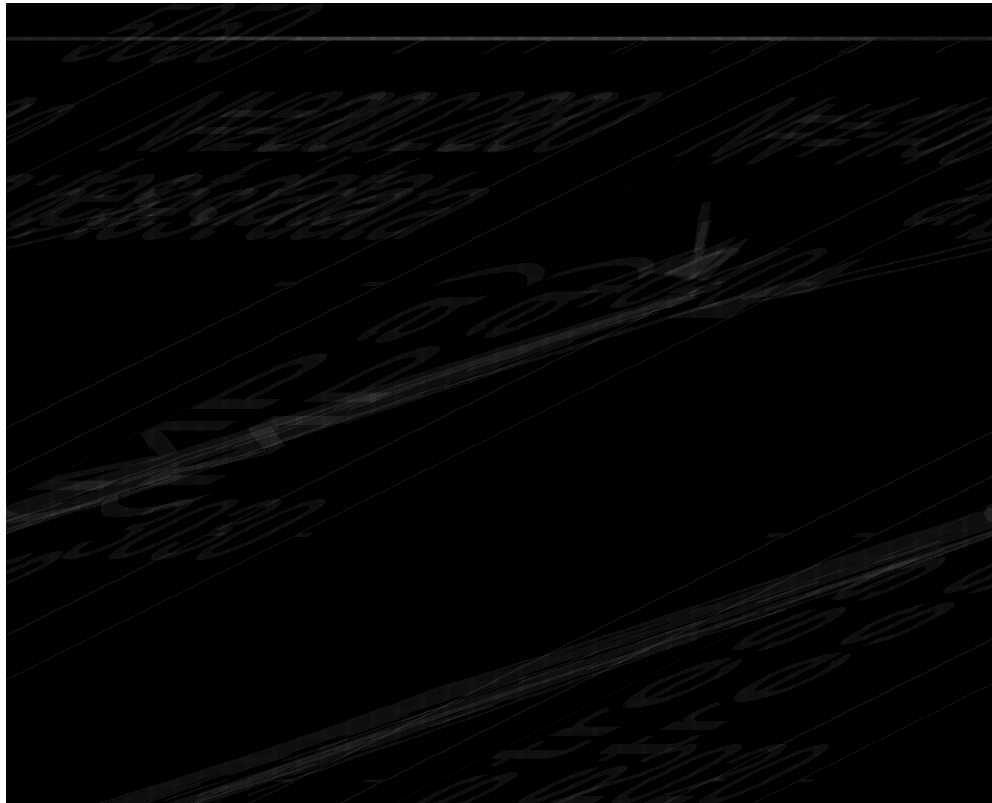


Figure 7 Stress-controlled proportional (equi-biaxial) cyclic loading with stress range of $\Delta\sigma_a = \Delta\sigma_h = 40$ MPa: (a) experimental axial stress-strain response, (b) experimental hoop stress-strain response, (c) predicted axial stress-strain response and (d) predicted hoop stress-strain response.

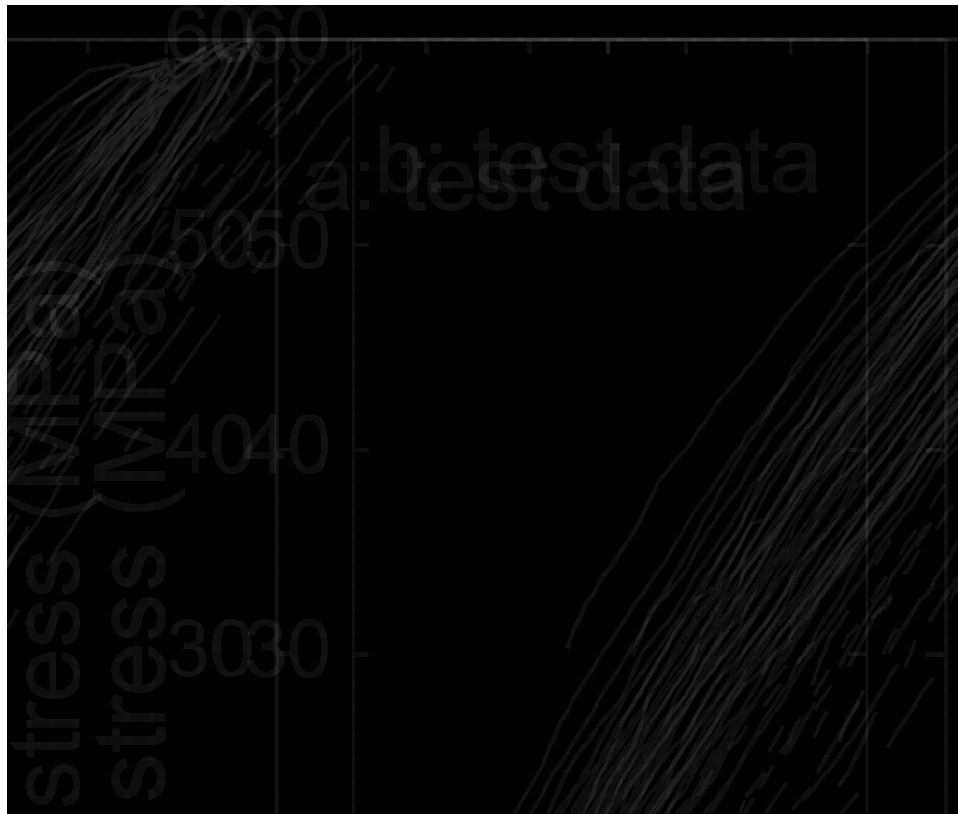


Figure 8 Stress-controlled proportional (equi-biaxial) cyclic loading with stress range of $\Delta\sigma_a = \Delta\sigma_h = 60$ MPa: (a) experimental axial stress-strain response, (b) experimental hoop stress-strain response, (c) predicted axial stress-strain response and (d) predicted hoop stress-strain response.



Figure 9 The first, the sixtieth and the seventieth hysteresis loops of stress-controlled proportional (equi-biaxial) cyclic loading with stress range of $\Delta\sigma_a = \Delta\sigma_h = 60$ MPa: (a) experimental axial stress-strain loops, (b) experimental hoop stress-strain loops, (c) predicted axial stress-strain loops and (d) predicted hoop stress-strain loops.

is, there is an evolution of hysteresis loops towards a slimmer stable shape.

3.3. Non-proportional quarter-circle sectorial cyclic loading under strain-control

Figs 10a, b and 11a, b show the hysteresis loops of the strain-controlled non-proportional cyclic loading with two different strain ranges, $\Delta\varepsilon_a = \Delta\varepsilon_h = 1.5\%$ and $\Delta\varepsilon_a = \Delta\varepsilon_h = 3\%$, respectively. As before, the first hysteresis loops and the last one prior to specimen failure with the higher strain range of $\Delta\varepsilon_a = \Delta\varepsilon_h = 3\%$ are depicted in Figs 12a and b for a better comparison.

From the above test results, it is noted that there is an anisotropy of stress-strain responses in axial and hoop directions induced by the non-proportional cyclic loading path. That is, the axial hysteresis loops are narrower in size than that of hoop ones, c.f. Figs 10a with b and 11a with b. This is particularly true with the high applied strain in Figs 11 and 12. In addition, the axial and hoop hysteresis loops rotate in opposite directions, i.e. axial loops rotate in the counter-clockwise while the hoop ones in the clockwise.

Under strain-controlled cyclic loading, the uncontrolled stress components gradually decrease in magnitude with the increasing number of cycles. They asymptotically reach a stable level after certain number of cycles ($N=100$ with the strain range of $\Delta\varepsilon_a = \Delta\varepsilon_h = 1.5\%$ and $N=20$ with that of

$\Delta\varepsilon_a = \Delta\varepsilon_h = 3\%$). In the case of the test with the strain range of $\Delta\varepsilon_a = \Delta\varepsilon_h = 3\%$, Fig. 13a depicts the cyclic strain path and Fig. 13b shows the cone-shaped stress responses in the $\sigma_a - \sigma_h$ stress plane.

3.4. Non-proportional quarter-circle sectorial cyclic loading under stress-control

Stress-controlled non-proportional cyclic tests with two different stress ranges, $\Delta\sigma_a = \Delta\sigma_h = 40$ MPa and $\Delta\sigma_a = \Delta\sigma_h = 60$ MPa, were performed. The hysteresis loops are shown in Figs 14a, b, and 15a, b. One observes the anisotropy of stress-strain responses in axial and hoop directions induced by the non-proportional cyclic loading path. Again, the axial and hoop hysteresis loops rotate in opposite directions. Under this loading condition, the uncontrolled strain components show a fan-shaped response in $\varepsilon_a - \varepsilon_h$ plane as portrayed in Fig. 16b.

With the small applied stress range in Figs 14a and b, a small ratcheting strain was accumulated in both axial and hoop directions. After about 200 cycles, a cyclic stable state was reached. The specimen did not fail even after 400 cycles. When the stress range was increased to $\Delta\sigma_a = \Delta\sigma_h = 60$ MPa, Figs. 15a and b, ratcheting became more significant, especially in the hoop direction. Due to the high cyclic stress range, the specimen failed after only 10 cycles. Neither a decreasing ratcheting rate nor a saturated stress-strain response was observed in this case.

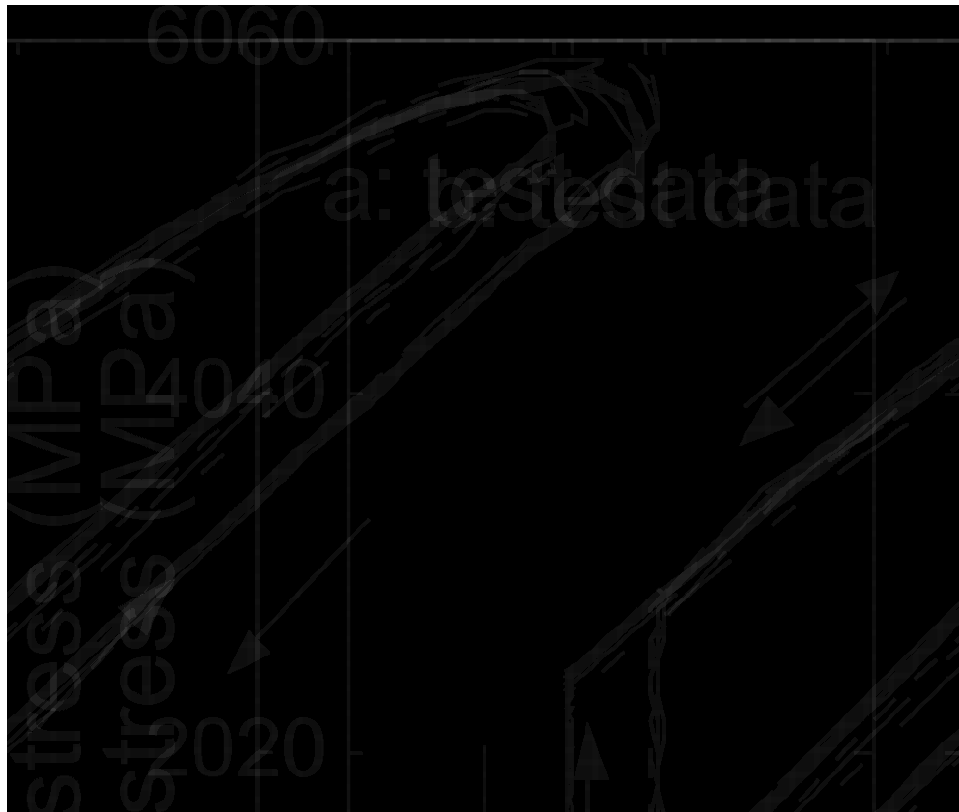


Figure 10 Strain-controlled non-proportional quarter-circle sectorial cyclic loading with strain range of $\Delta\varepsilon_a = \Delta\varepsilon_h = 1.5\%$: (a) experimental axial stress-strain response, (b) experimental hoop stress-strain response, (c) predicted axial stress-strain response and (d) predicted hoop stress-strain response.

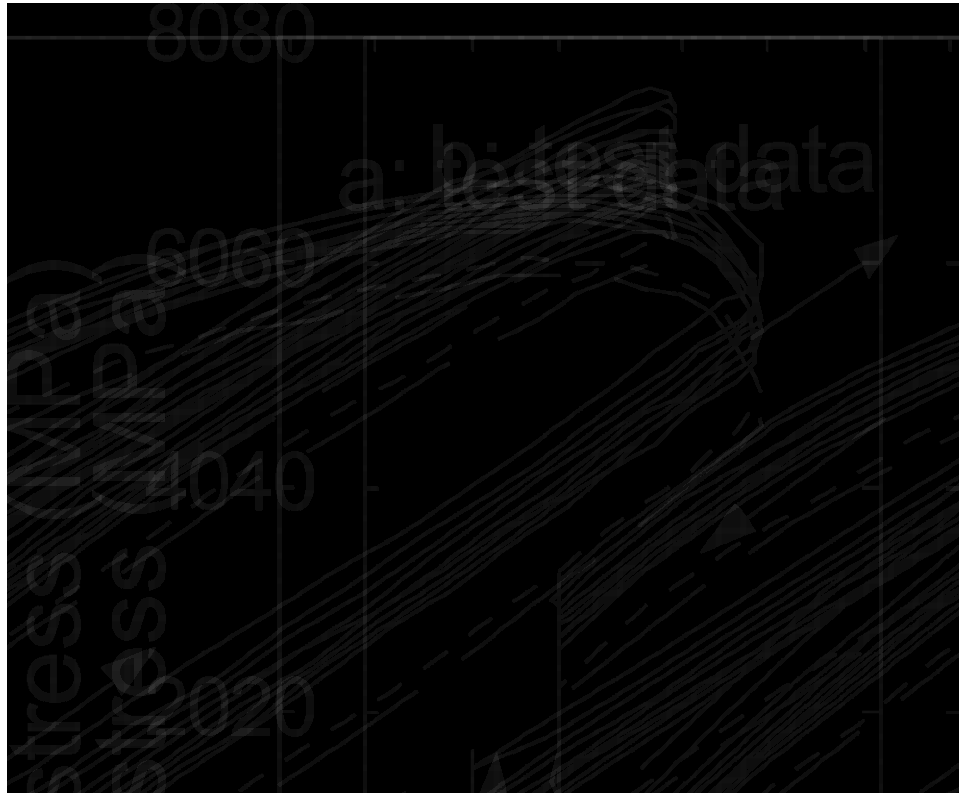


Figure 11 Strain-controlled non-proportional quarter-circle sectorial cyclic loading with strain range of $\Delta\varepsilon_a = \Delta\varepsilon_h = 3\%$: (a) experimental axial stress-strain response, (b) experimental hoop stress-strain response, (c) predicted axial stress-strain response and (d) predicted hoop stress-strain response.



Figure 12 The first and the twenty-fifth hysteresis loops of strain-controlled non-proportional quarter-circle sectorial cyclic loading with strain range of $\Delta\varepsilon_a = \Delta\varepsilon_h = 3\%$: (a) experimental axial stress-strain loops, (b) experimental hoop stress-strain loops, (c) predicted axial stress-strain loops and (d) predicted hoop stress-strain loops.

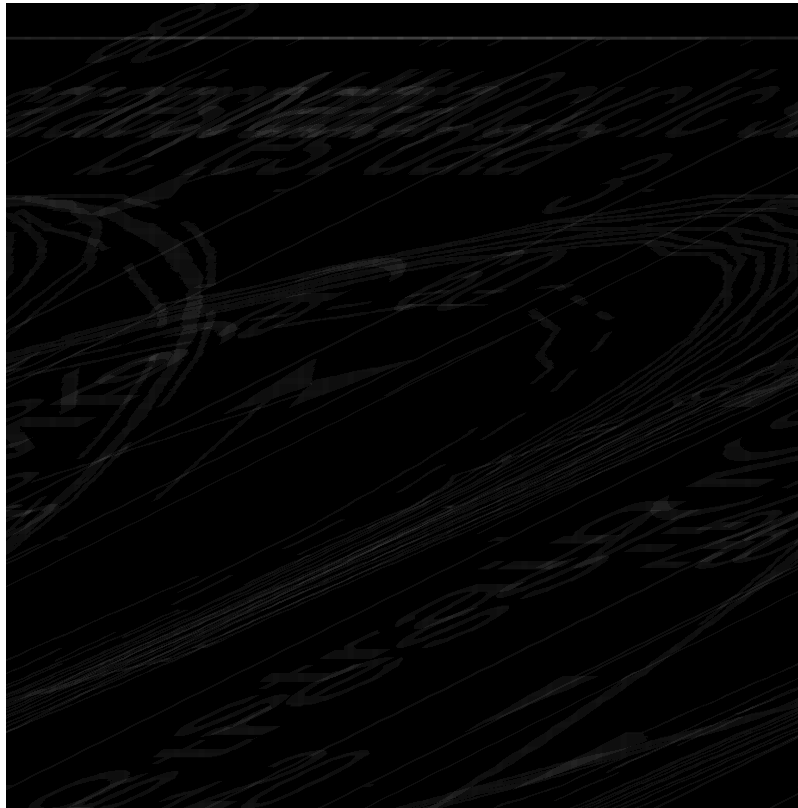


Figure 13 Strain-controlled non-proportional quarter-circle sectorial cyclic loading with strain range of $\Delta\varepsilon_a = \Delta\varepsilon_h = 1.5\%$: (a) experimental cyclic strain path, (b) experimental stress response and (c) predicted stress response.



Figure 14 Stress-controlled non-proportional quarter-circle sectorial cyclic loading with stress range of $\Delta\sigma_a = \Delta\sigma_h = 40$ MPa: (a) experimental axial stress-strain response, (b) experimental hoop stress-strain response, (c) predicted axial stress-strain response and (d) predicted hoop stress-strain response.



Figure 15 Stress-controlled non-proportional quarter-circle sectorial cyclic loading with stress range of $\Delta\sigma_a = \Delta\sigma_h = 60$ MPa: (a) experimental axial stress-strain response, (b) experimental hoop stress-strain response and (c) predicted axial stress-strain response, (d) predicted hoop stress-strain response.



Figure 16 Stress-controlled non-proportional quarter-circle sectorial cyclic loading with stress range of $\Delta\sigma_a = \Delta\sigma_h = 40$ MPa: (a) experimental cyclic stress path, (b) experimental strain response and (c) predicted strain response.

4. Constitutive modeling and predictions

4.1. Description of constitutive model

A recently proposed rheological nonlinear viscoelastic constitutive model was employed in this study to simulate the experimental observations. The fundamental equations of the constitutive model will be reviewed and a criterion to distinguish loading/unloading will be discussed. This criterion has been found to play an important role in simulating material behavior under cyclic loading, see ref. [18]. Other details of the constitutive model can be found in [3].

The model is in differential form. It can be viewed as a combination of one linear spring and several nonlinear Kelvin (Voigt) elements in series in its uniaxial representation. It is assumed that the total strain rate, $\{\dot{\varepsilon}_t\}$, is the sum of the elastic and the creep strain rates, $\{\dot{\varepsilon}_e\}$ and $\{\dot{\varepsilon}_c\}$, respectively, i.e.

$$\{\dot{\varepsilon}_t\} = \{\dot{\varepsilon}_e\} + \{\dot{\varepsilon}_c\} \quad (3)$$

The elastic strain rate is calculated through the generalized Hooke's law,

$$\{\dot{\sigma}\} = E[A]^{-1}\{\dot{\varepsilon}_e\} \quad (4)$$

where E is the elastic modulus, $[A]$ is a matrix related to the value of Poisson's ratio and defined by

$$[A] = \begin{bmatrix} 1 & -\nu & -\nu & 0 & 0 & 0 \\ -\nu & 1 & -\nu & 0 & 0 & 0 \\ -\nu & -\nu & 1 & 0 & 0 & 0 \\ 0 & 0 & 0 & 1 + \nu & 0 & 0 \\ 0 & 0 & 0 & 0 & 1 + \nu & 0 \\ 0 & 0 & 0 & 0 & 0 & 1 + \nu \end{bmatrix} \quad (5)$$

For a number of Kelvin (Voigt) elements connected in series, creep strain rate is the sum of the creep strain rate of each element, i.e.

$$\{\dot{\varepsilon}_c\} = \sum_{i=1}^n \{\dot{\varepsilon}_{ci}\} = \sum_{i=1}^n \left(\frac{[A]}{E_i \tau_i} \{\sigma\} - \frac{1}{\tau_i} \{\varepsilon_{ci}\} \right) \quad (6)$$

where $\tau_i = \eta_i/E_i$ denotes the retardation time, η_i is the dashpot viscosity and E_i is the spring stiffness for the i -th Kelvin (Voigt) element, respectively. It is to be noted that the retardation time τ_i in Equation 6 has a damped exponential character as in an exponential-type function. We further introduce a time scale factor α , and assume $\tau_i = (\alpha)^{i-1} \tau_1$. In this way all τ_i are related through the scale factor α .

To suit more general (proportional or non-proportional) cyclic loading paths, a rule to distinguish loading/unloading is further modified by defining a stress memory surface (Fig. 17):

$$f_m^\sigma(\sigma_{ij}) - R_{\max}^2 = \frac{3}{2} s_{ij} s_{ij} - R_{\max}^2 = 0 \quad (7)$$

where $s_{ij} = \sigma_{ij} - \frac{1}{3} \sigma_{kk}$ is the deviatoric stress components. The radius of the memory surface, R_{mem} , is de-



Figure 17 Schematic representation of a current memory surface and the loading/unloading criterion.

termined by the maximum von Mises equivalent stress level experienced by the material during its previous loading history, i.e. $R_{\text{mem}} = \sqrt{(\frac{3}{2} s_{ij} s_{ij})_{\max}}$. The following rules are adopted:

- if the current stress point is *on the memory surface* and $(\frac{\partial f}{\partial \sigma_{ij}})_{\sigma_{ij}^t} \cdot d\sigma_{ij}^t \geq 0$, this signifies a loading case;
- if the current stress point is *on the memory surface* and $(\frac{\partial f}{\partial \sigma_{ij}})_{\sigma_{ij}^t} \cdot d\sigma_{ij}^t < 0$, then a switch from loading to unloading occurs;
- if the current stress point is *inside the memory surface*, i.e. $f_m^\sigma(\sigma_{ij}^t) - R_{\max}^2 < 0$, it is then an unloading case.

For the loading case the spring stiffness of all the Kelvin elements is defined as a function of the equivalent stress, $E_i = E_1(\sigma_{\text{eq}})$. For the unloading case, it is assumed that E_i remains the same value during the entire unloading process, which is equal to the value of E_1 at the switch point, where unloading takes place.

The detailed procedure for the determination of the material constants and the modulus function can be found in ref. [3]. The anisotropy between tension and compression behavior of polymers is defined by R which is the ratio of the yield stress in compression to tension. The parameters used in this study are listed as follows:

$$\begin{aligned} E &= 2800 \text{ MPa}, & \nu &= 0.42, & \alpha &= 10, \\ \tau_1 &= 6.116 \text{ s}, & R &= 1.15, & n &= 6 \text{ and} \\ E_1(\sigma) &= 1.055 \times 10^5 e^{-\frac{\sigma-22.764}{18.000}} \text{ MPa} \end{aligned}$$

4.2. Comparison with experimental data

The predicted stress-strain loops for the equi-biaxial strain-controlled loading conditions are depicted in Figs 3c, d, 4c, d and 5c, d. The model predicts a mean stress relaxation in both axial and hoop directions. Quantitative comparison also shows a good agreement with the experimental data. As mentioned earlier, for

the cyclic test with a mean stress or mean strain, the specimen was first loaded to the mean stress or mean strain level and thereafter cyclic loading commenced. Hence, in the Figs 4 and 5, for example, the cycling process starts at the mean strain value of 1.5%, while the model predictions always start at the stress-free (virgin) state.

Figs 7–9 compares the experimental data with the predictions of the constitutive model in the case of stress-controlled equi-biaxial cyclic loading. It is observed that the constitutive model simulated well the ratcheting behavior, i.e. with the increasing number of cycles, the predicted ratcheting rate decreases and the stress-strain hysteresis loops gradually reach a saturated state, a phenomenon observed by experiments, c.f. Figs 7c, d with 7a, b, and 8c, d with 8a, b. The predicted magnitudes of accumulated ratcheting strains are comparable with the experimental data. In addition, the predicted stress-strain evolution process, i.e. hysteresis loops becoming slimmer with cycling, is also consistent with the experimental observations, c.f. Figs 9c, d with 9a, b.

The predictions of the non-proportional strain-controlled cyclic loading are depicted in Figs 10–13. In contrast to the proportional (equi-biaxial) loading, one notes two different manifestations induced by the non-proportional cyclic path: (a) the axial and hoop stress-strain loops are different in size and shape, and; (b) the axial and hoop hysteresis loops rotates in opposite directions. The constitutive model did predict the above two characteristics for this non-proportional loading path. The model also correctly simulated the decrease of stress values with the increasing cycles, and the predicted magnitude of reduction of stress components was very close to the experimental data, c.f. Figs 12c, d with 12a, b.

In the case of non-proportional cyclic loading under stress-controlled mode, Figs 14–16, the predictions by the constitutive model are also satisfactory both with respect to the primary stress-strain responses (size and shape of hysteresis loops) and the ratcheting behavior. It should be pointed out that for the stress range of $\Delta\sigma_a = \Delta\sigma_h = 60$ MPa, Fig. 15, the stress range in hoop direction of the first cycle in test, Fig. 16b, was approximately 53 MPa, below the desired value of 60 MPa, but it was subsequently corrected to achieve the desired value. The model prediction for the hoop direction in this case was simulated exactly as the experimental loading conditions.

5. Conclusions

From the results of biaxial cyclic tests and the comparison of the constitutive model predictions with the test data, the following conclusions are drawn:

- Under strain-controlled proportional (equi-biaxial) cyclic loading with mean strain, there is a mean stress relaxation in both axial and hoop directions. The mean stress of the cyclic straining as well as the hysteresis loops reaches a stable state with increasing number of cycles.
- Under stress-controlled proportional (equi-biaxial) cyclic loading with a mean stress, ratcheting strains are accumulated in both axial and hoop directions. The ratcheting rate decreases with the increasing number of cycles and the hysteresis loops become slimmer and less nonlinear until the attainment of a cyclic stable state.
- Under non-proportional cyclic loading path, anisotropy in stress-strain responses in the axial and hoop directions is noted and these hysteresis loops rotate in opposite directions. Under strain-controlled cyclic loading, the uncontrolled stress components gradually decrease in magnitude with the increasing number of cycles. They asymptotically reach a stable level after certain number of cycles. Under stress-controlled cyclic loading, a mean stress relaxation occurs in both axial and hoop directions.
- Test results were used to verify the predictive capabilities of a constitutive model. This comparison indicated that the constitutive model is capable of simulating most experimental observations, e.g. mean stress relaxation and ratcheting strain accumulation. Even in the case of complex non-proportional cyclic loading paths, the constitutive model simulated quite well the experimental results qualitatively and quantitatively.

Acknowledgement

The work presented here is part of a general investigation of the mechanical properties and damage prediction of composite materials. The research is supported, in part, by the Natural Sciences and Engineering Research Council of Canada (NSERC) through grants to Z.X. and F.E.

References

1. K. W. LOH, A. A. O. TAY and S. H. TEOH, *Polym. Eng. Sci.* **36** (1996) 1990.
2. Y. OCSUKI, T. KAJIWARA and K. FUNATSU, *ibid.* **39** (1999) 1969.
3. Z. XIA, Y. HU and F. ELLYIN, *ibid.* **43** (2003) 734.
4. C. ZHANG and I. D. MOORE, *ibid.* **37** (1997) 414.
5. J. LAI and A. BAKKER, *Comput. Mech.* **18** (1996) 182.
6. A. D. DROZDOV and A. L. KALAMKAROV, *Polym. Eng. Sci.* **36** (1996) 1907.
7. R. A. SCHAPERLY, *Int. J. Solids & Structures* **37** (2000) 359.
8. Y. HU, Z. XIA and F. ELLYIN, *Polym. Eng. Sci.* **43** (2003) 721.
9. X. SHEN, Z. XIA and F. ELLYIN, *ibid.* (accepted).
10. Y. JIANG and H. SEHITOGLU, *Int. J. Plast.* **10** (1994) 579.
11. Z. XIA and F. ELLYIN, *J. Appl. Mech.* **58** (1991) 317.
12. G. MEIJER, Z. XIA and F. ELLYIN, *Acta Mater.* **45** (1997) 3237.
13. S. RABINOWITZ and P. BEARDMORE, *J. Mater. Sci.* **9** (1974) 81.
14. D. J. KIZYPOW and C. M. RIMNAC, *Biomaterials* **21** (2000) 2081.
15. T. ARIYAMA, *Polym. Eng. Sci.* **33** (1993) 18.
16. R. J. SCAVUZZO, *J. Press. Vesel Tech.* **122** (2000) 386.
17. F. ELLYIN, in "Fatigue Damage, Crack Growth, and Life Prediction" (Chapman & Hall, London, 1997) p.179.
18. Z. XIA, X. SHEN and F. ELLYIN, *Polym. Eng. Sci.* (accepted).

Received 26 April
and accepted 24 September 2004